Experimental Neurology 352 (2022) 114031

Contents lists available at ScienceDirect

Experimental Neurology

journal homepage: www.elsevier.com/locate/yexnr

Review article

Electrophysiological characterization of the hyperdirect pathway and its functional relevance for subthalamic deep brain stimulation

Bahne Hendrik Bahners [a], Gunnar Waterstraat [b], Silja Kannenberg [a], Gabriel Curio [b,c], Alfons Schnitzler [a,d], Vadim Nikulin [e], Esther Florin [a,*]

[a] Institute of Clinical Neuroscience and Medical Psychology, Medical Faculty, Heinrich-Heine-University, Düsseldorf, Germany
[b] Charité – Universitätsmedizin Berlin, corporate member of Freie Universität Berlin and Humboldt-Universität zu Berlin, Neurophysics Group, Department of Neurology, Berlin, Germany
[c] Bernstein Center for Computational Neuroscience, Berlin, Germany
[d] Department of Neurology, Center for Movement Disorders and Neuromodulation, Medical Faculty, Heinrich-Heine-University, Düsseldorf, Germany
[e] Department of Neurology, Max Planck Institute for Human Cognitive and Brain Sciences, Leipzig, Germany

ARTICLE INFO

Keywords:
High frequency oscillations
Stimulation evoked responses
Antidromic activation
Signal-to-noise ratio

ABSTRACT

The subthalamic nucleus (STN) receives input from various cortical areas via hyperdirect pathway (HDP) which bypasses the basal-ganglia loop. Recently, the HDP has gained increasing interest, because of its relevance for STN deep brain stimulation (DBS). To understand the HDP's role cortical responses evoked by STN-DBS have been investigated. These responses have short (<2 ms), medium (2–15 ms), and long (20–70 ms) latencies. Medium-latency responses are supposed to represent antidromic cortical activations via HDP. Together with long-latency responses the medium responses can potentially be used as biomarker of DBS efficacy as well as side effects. We here propose that the activation sequence of the cortical evoked responses can be conceptualized as high frequency oscillations (HFO) for signal analysis. HFO might therefore serve as marker for antidromic activation. Using existing knowledge on HFO recordings, this approach allows data analyses and physiological modeling to advance the pathophysiological understanding of cortical DBS-evoked high-frequency activity.

1. Introduction

The subthalamic nucleus (STN) receives both indirect cortical input via the basal-ganglia loops (Albin et al., 1989; DeLong, 1990) as well as direct excitatory input from layer V cortical neurons (Coudé et al., 2018; Hartmann-von Monakow et al., 1978; Haynes and Haber, 2013; Nambu et al., 1996). This latter pathway has been termed the cortico-subthalamic hyperdirect pathway (HDP) due to bypassing the striatum. A number of studies have argued that HDP activation is key for STN-DBS efficacy (Anderson et al., 2018; Chen et al., 2020; Gradinaru et al., 2009; Kuriakose et al., 2010; Li et al., 2012; Miocinovic et al., 2018; Sanders and Jaeger, 2016; Walker et al., 2012a), suggesting the HDP's involvement in the pathology of Parkinson's disease (PD). The main physiological role of the HDP seems to be action inhibition (Chen et al., 2020; Gradinaru et al., 2009; Gurney et al., 2001; Nambu, 2005).

Historically, descriptions of such cortical projections to the STN had already been made at the end of the 1930s and were reported in non-human primates (NHP) in 1978 (Hartmann-von Monakow et al., 1978). In humans, electrophysiological evidence for hyperdirect cortical projections derives from DBS evoked cortical responses (eCR). These eCR occur as a sequence, with initial latencies as short as 1 ms, followed by components with a periodicity of ~2 ms, suggesting antidromic activation of the HDP (Chen et al., 2020; Hartmann et al., 2018; Miocinovic et al., 2018; Walker et al., 2012a). For the purpose of signal analysis, such eCR sequences can be treated as a particular case of high-frequency oscillations (HFO) rather than a sequence of separate peaks. HFO analysis could then be fruitfully employed to first characterize the HFOs due to STN-DBS and to then discriminate antidromic activation from orthodromic effects, effectively creating a biomarker of antidromic activation. While theoretically straightforward, detecting HFOs is practically very challenging with standard EEG or MEG paradigms, because the signal-to-noise ratio (SNR) of the HFO is low. We will therefore provide guidelines on how to detect HFOs in such setups.

We start this review by first summarizing current studies on the HDP

* Corresponding author at: Heinrich-Heine University Düsseldorf, Institute of Clinical Neuroscience and Medical Psychology, Universitätstr. 1, 40225 Düsseldorf, Germany.
E-mail address: Esther.Florin@hhu.de (E. Florin).

https://doi.org/10.1016/j.expneurol.2022.114031
Received 31 March 2021; Received in revised form 1 February 2022; Accepted 28 February 2022
Available online 2 March 2022

in humans and animals in Section 2. In Section 3 we will discuss both the physiological and the pathological role of the HDP. In Section 4, we will argue that post-DBS-eCRs should be analyzed as HFO and provide guidelines on how to record and extract such HFO non-invasively.

2. Anatomical and electrophysiological characterization of the HDP

The first anatomical studies using radiographic tracing in NHP investigated frontal and precentral cortical connections to the STN and described a somatotopic organization of these pathways (Hartmann-von Monakow et al., 1978; Künzle, 1978). While the lateral STN receives direct input from the primary motor cortex (M1), the medial STN receives projections from the supplementary motor area (SMA) (Nambu et al., 1997, 1996). M1 innervation of the STN originates from corticofugal axons with a diameter of 2–3 μm in NHP, which in turn give rise to collaterals of 0.5–1.5 μm that form synapses with the sensorimotor subregion of STN (Coudé et al., 2018). In addition, the primary somatosensory region (S1) and the prefrontal cortex (PFC) project to the STN (Canteras et al., 1990, 1988; Haynes and Haber, 2013). All of these connections are part of the cortico-subthalamic HDP. In humans, the HDP has been identified anatomically using MRI tractography (Akram et al., 2017; Chen et al., 2018; Petersen et al., 2017; Plantinga et al., 2016).

In line with those anatomical studies, electrophysiological studies also indicate the existence of cortico-STN projections and STN subsections (Giuffrida et al., 1985; Kitai and Deniau, 1981; Maurice et al., 1998; Rouzaire-Dubois and Scarnati, 1985). PFC stimulation in rats leads to excitation of medial STN neurons (Maurice et al., 1998). Conversely, the stimulation of medial STN neurons leads to an antidromic spike in layer V neurons of the PFC at a latency of 2 to 9 ms (Maurice et al., 1998), consistent with studies indicating that cortico-STN projections originate in layer V (Donoghue and Kitai, 1981; Giuffrida et al., 1985; Kumaravelu et al., 2018).

Various studies have investigated the HDP's existence in rodents by stimulating within the STN (Dejean et al., 2009; Devergnas and Wichmann, 2011; Kumaravelu et al., 2018; Li et al., 2007), reporting eCRs in a range of 1.4 to 2.5 ms. Corticospinal tract (CST) stimulation in rats led to eCRs with similar latencies as STN stimulation (Porter and Sanderson, 1964), suggesting that corticospinal collaterals projecting to the STN can account for the eCR latencies of 1.4–2.5 ms (Kita and Kita, 2012; Li et al., 2007). Results from 6-OHDA lesioned rats suggest that eCRs are not influenced by substantia nigra (SN) dopaminergic degeneration (Kumaravelu et al., 2018), whereas a recent study in NHP found that

Table 1
Overview of EP latencies in PD, essential tremor and dystonia.

Authors	Target	Short latency (ms)	Medium latency (ms)				Long latency (ms)				Sampling rate (kHz)	Low-pass filter (kHz)
		EP0/R1	EP1	EP2a	EP2b/ R2	EP3	T1/R3	P1	T2	P2		
Limousin et al. (1998)	STN						19.0 ± 1.0					
Ashby et al. (2001)	STN			3.3 ± 0.5	5.4 ± 0.9	7.5 ± 0.7						1.0
Baker et al. (2002)	STN	1.0–2.0			8.0	14.0	29.0			70	0.6	0.25
MacKinnon et al. (2005)	STN					12.5 ± 2.2	23.2 ± 3.7				5.0	1.0
Eusebio et al. (2009)	STN						21.4 ± 1.9				1.5	0.3
Kuriakose et al. (2010)	STN			3.7 ± 0.6		7.4 ± 0.9	22.2 ± 1.2				5.0	0.5
Walker et al. (2012a)	STN	1 ± 0.4			5.7 ± 1.1	10.0 [3]	22.2 ± 1.8				10.0	3.0
Miocinovic et al. (2018)	STN	1.5 ± 0.1	2.8 ± 0.3 [1]		5.8 ± 1.0 [1]	7.7 ± 1.8	20 ± 8	38 ± 11	56 ± 15	71 ± 16	22.0	3.5
			2.3 ± 0.2 [2]	4.1 ± 0.6 [2]							24.42	10.0
Hartmann et al. (2018)	STN	~ 1		4 ± 0		11 ± 1	27 ± 6				5.0	
Romeo et al. (2019)	STN	0.89 ± 0.09					20				25.0	10.0
Chen et al. (2020)	STN		2.2 ± 0.2		6.0 ± 0.35						22.0	3.5
Irwin et al. (2020)	STN	0.5–1.4 [4]			R2		R3				50.0	10.0
Limousin et al. (1998)	GP						25.4 ± 0.4					
Tisch et al. (2008)	GP					10.9 ± 0.77	26.6 ± 1.6					
Bhanpuri et al. (2014)	GP						20 ± 8					
Ni et al. (2018)	GP					10	25					
Miocinovic et al. (2018)	GP	1.5 ± 0.1				10 ± 2 [3]	19 ± 3	29 ± 4	44 ± 9		22.0	3.5
Limousin et al. (1998)	VIM					8.2	15.1 ± 0.3					
Walker et al. (2012b)	VIM	0.9 ± 0.2	2.6 ± 0.5		5.6 ± 0.7	8.6 ± 0.8	13.9 ± 1.4				10.0	3.0
Hartmann et al. (2018)	VIM	~ 1					13 ± 1	40 ± 9	77 ± 13	116 ± 13	5.0	

[1] latency over M1,
[2] latency over S1.
[3] value estimated visually from plot.
[4] latency depending on anaesthesia state and stimulation voltage.

especially long-latency eCRs become progressively delayed with advancing Parkinsonian state (Campbell et al., 2021).

In humans, the HDP can be antidromically activated via DBS (Chen et al., 2020; Hartmann et al., 2018; Irwin et al., 2020; Miocinovic et al., 2018; Romeo et al., 2019; Walker et al., 2012a). The findings of the different studies on eCR latencies for humans are summarized in Table 1 and are discussed within the remainder of this section. In general, eCR due to STN-DBS result in short-latency (<2 ms), medium-latency (2–15 ms), and long-latency (20–70 ms) responses (Miocinovic et al., 2018; Walker et al., 2012a), each of which can be linked to a different transmission pathway. As illustrated in Fig. 1 eCR latencies can be attributed to either antidromic hyperdirect or CST activation and recent work has focused on electrophysiologically differentiating these two pathways (Hartmann et al., 2018; Miocinovic et al., 2018; Walker et al., 2012a). This differentiation has even been used to validate connectome modeling studies (Howell et al., 2021).

Short-latency EP as reported in most recent STN-DBS studies (Table 1) are thought to result from activation of pyramidal fiber tracts (Irwin et al., 2020; Miocinovic et al., 2018). These short-latency responses are mainly located within primary motor areas, whereas later responses exhibit a broader cortical distribution (Miocinovic et al., 2018). The short-latency EP can also be observed for pallidal and thalamic DBS (Hartmann et al., 2018; Miocinovic et al., 2018; Walker et al., 2012b), where the target areas are in close proximity to the internal capsule. Short-latency eCR may therefore be caused by stimulation current spreading to the large diameter pyramidal fibers of the internal capsule (Miocinovic et al., 2018; Walker et al., 2012a). Short-latency EP are less variable in timing than the later responses (Walker et al., 2012a) and are accompanied by motor evoked potentials (MEP) in most of the studies co-registering electromyography (EMG) (Ashby et al., 2001; Irwin et al., 2020; Miocinovic et al., 2018). Moreover, if the first eCR has a very short latency (<1 ms), this is indicative of motor side effects (Irwin et al., 2020). This relationship between MEP and eCR further supports the idea that cortical responses at short latencies occur due to CST activation (Irwin et al., 2020; Miocinovic et al., 2018).

According to a computational model, a conduction velocity of 85 m/s with fiber diameters of 15 μm is necessary to explain an antidromic activation of layer V pyramidal neurons at 1.5 ms, implying that earlier cortical responses are incompatible with action potential biophysics (Gunalan and McIntyre, 2020). Still, several human studies report short-latency eCR of less than 1.5 ms and in some the eCR latency and amplitude correlate with clinical effects (Hartmann et al., 2018; Irwin et al., 2020; Romeo et al., 2019; Walker et al., 2012a). Nevertheless, eCR at latencies of less than 1 ms may represent a volume-conducted signal from the STN rather than cortical activation, because large-amplitude activity (termed evoked resonant neural activity, ERNA) occurs locally during STN-DBS at short latencies of 0.3 ms (Awad et al., 2021; Gunalan and McIntyre, 2020; Sinclair et al., 2018).

Medium-latency eCR due to STN-DBS are considered

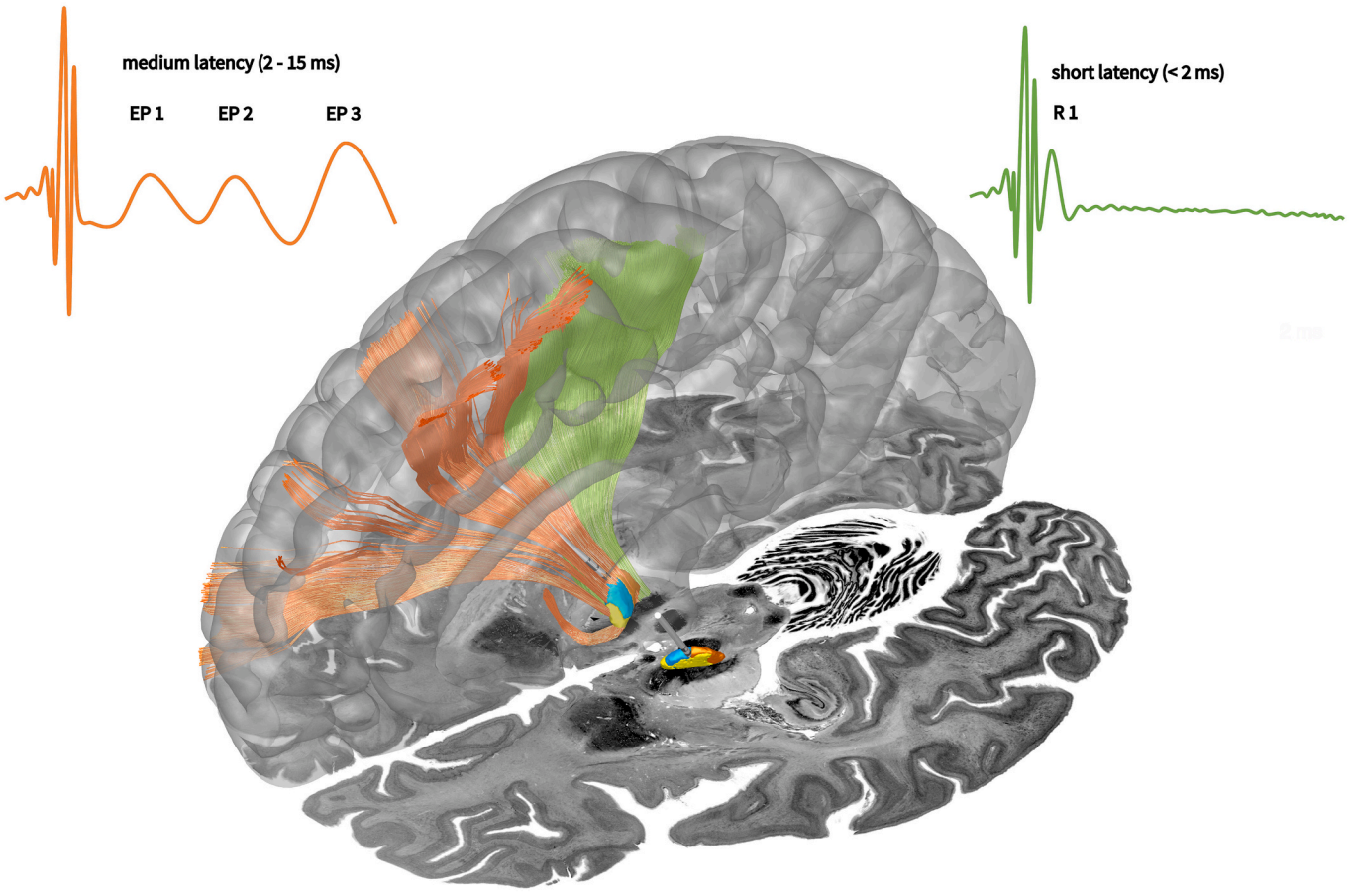

Fig. 1. Medium-latency evoked cortical responses (eCR) (top left, orange) result from hyperdirect pathway (HDP, orange fibers) activation. Short-latency eCR (top right, green) originate from corticospinal tract (CST, green fibers) activation. Orange and green eCR example traces are schematic drawings that do not refer to any particular recording modality. Example electrode trajectories inside the subthalamic nucleus (STN) and cortical surface were visualized using Lead-DBS (lead-dbs.org, RRID:SCR_002915) (Horn and Kühn, 2015). Subsections of the STN colored in orange (motor), blue (associative) and yellow (limbic) as well as fiber tracts of HDP (orange) and CST (green) were visualized with subcortical atlases pre-installed in Lead-DBS (Ewert et al., 2018; Meola et al., 2016; Middlebrooks et al., 2020). All structures are overlaid an axial section of the BigBrain dataset (Amunts et al., 2013) at z = −12 mm. (For interpretation of the references to color in this figure legend, the reader is referred to the web version of this article.)

electrophysiological evidence for antidromic HDP activation (Chen et al., 2020; Eusebio et al., 2009; Miocinovic et al., 2018). Given a fiber diameter of 5.7 to 10 μm and conduction velocities of 25 to 55 m/s, computational modeling supports hyperdirect activation leading to eCR at latencies of 3 to 5 ms (Gunalan and McIntyre, 2020). Additionally, medium-latency responses were not observed with pallidal and thalamic stimulation (Bhanpuri et al., 2014; Devergnas and Wichmann, 2011; Limousin et al., 1998; Miocinovic et al., 2018; Ni et al., 2018; Tisch et al., 2008), with one notable exception (Walker et al., 2012b). The absence of medium-latency eCR for pallidal stimulation indicates that they are likely to represent HDP activation (Miocinovic et al., 2018), which would also be consistent with the broad cortical distribution of medium-latency eCR (Canteras et al., 1988; Miocinovic et al., 2018; Nambu et al., 1997).

Most electrocorticography studies were able to detect three separate medium-latency eCR (Ashby et al., 2001; Chen et al., 2020; Miocinovic et al., 2018) (Table 1). While most EEG and MEG studies employing a low sampling rate do not report a third medium-latency response (Baker et al., 2002; Hartmann et al., 2018; Kuriakose et al., 2010; MacKinnon et al., 2005; Walker et al., 2012a), a third medium response became apparent with EEG with a high sampling rate (>20 kHz) (Irwin et al., 2020; Romeo et al., 2019). A necessity to have such high sampling frequency in order to see eCR, further validates the idea to conceptualize a sequence of evoked responses as HFO. The three separate medium-latency eCR may reflect the activation of hyperdirect fiber bundles with different diameters (Gunalan and McIntyre, 2020; Miocinovic et al., 2018). Alternatively, the second and third medium-latency responses may be caused by cortico-cortical synaptic transmission (Miocinovic et al., 2018).

A potential caveat when analyzing medium-latency eCR is scalp EMG activity (Romeo et al., 2019). MEP for facial muscles occur with a similar latency as medium-latency eCR (Mahlknecht et al., 2017; Miocinovic et al., 2018) and thus could be mistaken for medium-latency eCR due to subcortical stimulation. Still the medium-latency eCR is captured mainly by parietal EEG channels ipsilateral to the stimulation target (Romeo et al., 2019). On the other hand, the corticobulbar tract innervates cranial muscles bilaterally, so unilateral stimulation can evoke bilateral MEP. Therefore, controlling for this potential source of spurious cortical response by recording facial EMG is recommended.

Finally, long-latency responses around 20 ms are consistently found in most studies on STN and pallidal DBS (Table 1). These long-latency eCR might represent orthodromic synaptic transmission in the basal ganglia (BG)-thalamo-cortical loop (Miocinovic et al., 2018). However, a study combining computational modeling with a rodent model of PD argues that these long-latency eCR reflect cortico-thalamo-cortical synaptic transmission rather than the BG-thalamo-cortical loop (Kumaravelu et al., 2018).

3. The HDP's relevance for DBS and physiological function

The HDP is involved in both physiological cortical functions as well as PD pathophysiology. Human and animal studies attribute its physiological function to action inhibition (Chen et al., 2020; Gradinaru et al., 2009; Gurney et al., 2001; Nambu, 2005). The HDP significantly modulates the temporal dynamics of motor planning through global inhibition (Kumaravelu et al., 2018). In humans, synchronization between the STN and inferior frontal gyrus predicts stopping speed, indicating that prefrontal-STN projections modulate rapid inhibition (Chen et al., 2020). However, the HDP is also involved in PD pathophysiology. M1-STN connectivity as determined with tractography relates to tremor, whereas SMA-STN connectivity strength relates to bradykinesia and rigidity (Akram et al., 2017). Given the diverse role of the HDP found in these studies, the wide array of STN-DBS effects may not be surprising.

Activation of the HDP via high-frequency stimulation is considered an important mechanism of STN-DBS (Anderson et al., 2018; Chen et al., 2020; Gradinaru et al., 2009; Kuriakose et al., 2010; Miocinovic et al., 2018; Walker et al., 2012a). A computational model suggests that DBS causes functional disconnection of the cortex from the STN, reducing motor inhibition as well as the cortical generation and propagation of pathological oscillatory activity (Anderson et al., 2018). Antidromic activation of the HDP reduces cortical beta oscillations in rodents and is associated with therapeutic effects in PD rodent models (Dejean et al., 2009; Gradinaru et al., 2009; Sanders and Jaeger, 2016). Similarly, the antidromic spiking of layer V cortical M1 neurons positively correlates with reduced Parkinsonian symptoms in 6-OHDA rats (Li et al., 2012). At the same time, functional disconnection of hyperdirect cortical projections to the STN seems to not mono-causally explain therapeutic effects. For example the therapeutic effect of DBS remains in 1-methyl-4-phenyl-1,2,3,6-tetrahydropyridine (MPTP) treated NHP even though antidromic M1 activation fades after an interval of 4 h (Johnson et al., 2020). Moreover, pallidal DBS has similar effects on motor symptoms in PD, but does not involve stimulating the HDP (Miocinovic et al., 2018).

Latencies and amplitudes of eCR at short (<2 ms), medium (2 to 7 ms), and long (> 20 ms) latencies have shown some predictive power for the therapeutic effects of DBS. The amplitude of short-latency eCR due to STN stimulation over the ipsilateral sensorimotor cortex is non-linearly modulated by the underlying stimulation voltage (Walker et al., 2012a). These short-latency eCR also predict the occurrence of motor side effects and co-occur with MEP (Irwin et al., 2020), consistent with the eCR's generation from current spread to pyramidal fibers at higher stimulation amplitudes (Miocinovic et al., 2018). Such current spread to pyramidal fibers is well-known to cause motor side effects (Dembek et al., 2017). Due to its relation to DBS side effects, occurrence of MEPs may be able to guide electrode placement (Nikolov et al., 2021; Shils et al., 2021). With respect to medium-latency eCRs, highest amplitudes are elicited by clinically-used 130 Hz DBS stimulation (Miocinovic et al., 2018). This conforms well to GPi stimulation results in adult and adolescent dystonia patients where the amplitude of eCR around 20 ms correlates with the clinically most effective contact inside the GPi (Bhanpuri et al., 2014; Tisch et al., 2008). Finally, turning to longer latency eCRs, a large amplitude at about 20 ms following STN-DBS in PD patients is predictive for postoperative motor side effects (Romeo et al., 2019). Given the relationship between eCR and DBS (side) effects, future clinical research should focus on the applicability of eCR as therapeutic markers for optimized DBS.

Even though only high-frequency DBS elicits a therapeutic effect, there is a relationship between the amplitude of cortical responses evoked by low-frequency – non-effective – stimulation and the best clinical contact as assessed at high-frequency therapeutic DBS (Miocinovic et al., 2018). The responses with a clinical relationship had a latency of less than 3 ms (namely EP1, 2-3 ms, see Table 1) and therefore occur within the inter-pulse interval of therapeutic 130 Hz DBS (Miocinovic et al., 2018). Moreover, according to the literature medium-latency eCR in the time range of the inter-pulse interval of a stimulation at 130 Hz (~7 ms) are similar for both, high- and low-frequency DBS (Miocinovic et al., 2018). Therefore, the analysis of short- and medium-latency eCR does not appear to be affected by the DBS frequency. Long-latency eCR, that occur after the therapeutic DBS inter-pulse interval, rather relate to the occurrence of motor side effects than therapeutic efficacy (Irwin et al., 2020; Romeo et al., 2019). So even though, long-latency eCRs do not reflect all mechanisms of high-frequency DBS, they still seem to represent valuable markers for contact selection (Irwin et al., 2020).

Besides eCR, several studies have investigated local STN, GPi and VIM responses which were evoked by the stimulation of the respective target (Awad et al., 2021; Ozturk et al., 2021; Sinclair et al., 2019, 2018). These stimulation-evoked local responses are either termed evoked compound activity (ECA) or evoked resonant neural activity (ERNA) and resemble a decaying oscillation following the DBS pulses (Ozturk et al., 2021; Sinclair et al., 2019). They have peak latencies of 0.3 and 4 ms respectively and show a decay frequency of about 300 Hz (Awad et al., 2021; Ozturk et al., 2021). While stimulating in the STN

and GPi evokes ERNA at short (0.3 ms) and medium latencies (4 ms), thalamic stimulation only evokes short-latency ERNA at 0.3 ms (Awad et al., 2021).

So far, it has not been investigated how these local STN and cortical responses after a DBS pulse relate to each other. The highest amplitude of both ERNA at 4 ms and eCR at 2 ms are observed when the stimulation is applied to the best clinical DBS contact (Miocinovic et al., 2018; Sinclair et al., 2018). Amplitude and frequency of ERNA even correlate with the improvement of bradykinesia and rigidity scores (Sinclair et al., 2019). Based on the temporal order ERNA might result from a returning, orthodromic activation from the cortex with a similar latency as the antidromic activation (EP1 ~ 2 ms) adding up to a peak latency of 4 ms for the ERNA (Gmel et al., 2015). This could explain that short latency responses both in STN and cortex are predictive of the best clinical contact (Miocinovic et al., 2018; Sinclair et al., 2018). To test this hypothesis combined STN LFP-EEG/MEG recordings during low and high-frequency DBS are needed.

4. Perspective on the analysis of cortical high-frequency activation and high gamma activity as proxy for spiking activity

4.1. Somatosensory evoked high-frequency oscillations – lessons learned from a model system

As described in the previous section STN stimulation leads to direct antidromic activation of the motor cortex, manifested in electrocorticographic recordings as a series of short- and medium-latency eCR (Miocinovic et al., 2018). The earliest of these eCR occurs at a latency of about 1 ms after the stimulus - incompatible with synaptic transmission - and is followed by a sequence of components lasting for about 2.5–3 cycles with a period length of ~2 ms. Similar eCR but with a less refined morphology were also observed in scalp EEG (Ashby et al., 2001; Walker et al., 2012a). While these eCRs comprise distinct components, using a signal-analysis perspective, such short-interpeak-latency sequence of activation can be conceptualized as high-frequency oscillation (HFO) with an energy peak at ~500 Hz, motivating the search for an experimental paradigm that helps optimizing the yield from such non-invasive high-frequency recordings.

Notably, while standard EEG and MEG recordings provide excellent time-resolved information on post-synaptic low-frequency neuronal mass activity <200 Hz, a critical shortcoming is their limited ability to reflect high-frequency activity (>200 Hz) reliably. One prominent

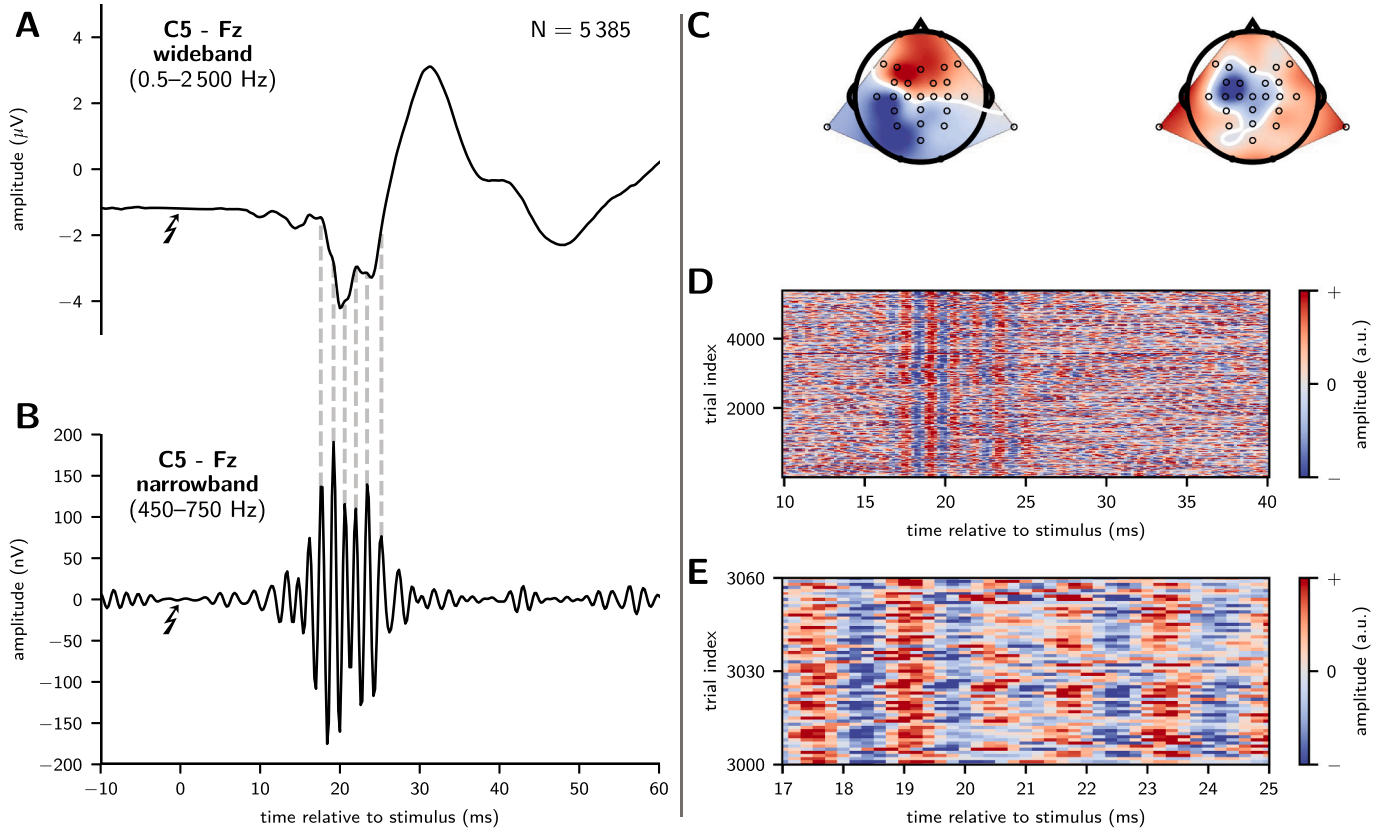

Fig. 2. High-frequency somatosensory evoked potentials, elicited by repetitive electric stimulation of the right median nerve at the wrist. (A): Averaged wideband responses ($N = 5385$) at electrode C5 with a reference at Fz show a negative peak at around 20 ms ("N20"). Notably, the slopes of that peak show a high-frequency series of humps and notches. (B): High-frequency somatosensory evoked potentials can be isolated by high-pass filtering around 600 Hz. The peaks and troughs of the resulting oscillation correspond to the humps and notches of the low-frequency response (dashed vertical lines), excluding an exclusive generation of the oscillation by filter artifacts. (C): Spatial decomposition of high-frequency somatosensory evoked potentials by Canonical Correlation Average Regression (cf. main text) depicts a bipolar source pattern across the left central sulcus (left), consistent with a tangential source in the somatosensory hand cortex (Brodmann Area BA 3b) and, additionally, a monopolar source pattern (right), consistent with radially oriented projections of thalamocortical afferents and/or a source in BA 1. (D): Single-trial response activity projected through the bipolar pattern in panel C (left) with polarity/amplitudes coded in color/saturation. (E) Zoom-in of panel D. Consecutive responses (ordinate) show significant variability with fluctuations of response latencies (abscissa) and, especially in the second half of the burst, partial reductions of response components.

exception has been characterized in the somatosensory system where a burst of averaged HFO (600–900 Hz) evoked by conventional repetitive electric peripheral nerve stimulation can be non-invasively detected (Fig. 2; Curio, 2000; Waterstraat et al., 2015a). Even though eCRs and somatosensory HFO do not reflect the same physiological mechanisms, similarities between eCRs and somatosensory HFO in terms of frequency, electric stimulus artifact, and spatially finite source origin render the analysis of non-invasive cortical 600 Hz-oscillations as optimal model paradigm for studying medium-latency eCRs.

Early MEG recordings proved that their generating source is located in S1 (Curio et al., 1994; Hashimoto et al., 1996), and subsequent studies in awake NHP demonstrated that these macroscopic HFO wavelets corresponded to synchronized evoked spike bursts as detected by simultaneous microelectrode recordings in an ensemble of single cells in S1 (Baker et al., 2003). Moreover, converging evidence from human non-invasive studies utilizing stimulus rate variations (Klostermann et al., 1999) and animal studies employing cortical applications of glutamate receptor antagonists (Ikeda et al., 2002) revealed that the 600 Hz HFO burst contained (i) early pre-synaptic components (reflecting repetitive population spikes ascending via thalamocortical fibers towards S1), and (ii) later wavelets contributed by a first-order post-synaptic intracortical population spiking of stimulus-driven neurons. Specifically, macroscopic EEG HFO-bursts were shown to covary with single-cell spike burst patterns simultaneously recorded in cortical S1 neurons (Teleńczuk et al., 2011), and synaptic refractoriness together with cortical excitability fluctuations were identified as critical components in a neurocomputational model explaining the observed variable spike burst responses in S1 (Teleńczuk et al., 2017). Although different parts of these oscillations in this context represent distinct neurophysiological processes, nonetheless signal analysis often conceptualizes the whole activation sequence as single HFO thus facilitating their temporal and spatial extraction – a similar idea is suggested here for the short- and medium-latency eCR in case of STN stimulation. Furthermore, recent improvements in reducing the white noise level in EEG as well as MEG recording systems have enabled the non-invasive detection of spike-like human somatosensory evoked responses in a frequency range even above 1 kHz, demonstrating a further step towards non-invasive multi-unit spike recordings (Fedele et al., 2015). Finally, these hardware refinements combined with tailor-made algorithmic tools (see below) permitted for the first time a non-invasive single-trial EEG detection of evoked human neocortical population spikes along with their variability over time (Waterstraat et al., 2015a, 2016, 2021). Thus, these accumulated experiences from somatosensory HFO recordings, data analyses and physiological modeling could be leveraged to advance the non-invasive detection and pathophysiological understanding of cortical DBS-evoked high-frequency activity.

4.2. High-frequency oscillations in the context of STN-DBS

According to a modeling study peaks of evoked responses observed at 2, 3 and 5 ms corresponded to the activation of axons with 15, 10 and 5.7 μm diameter, respectively (Gunalan and McIntyre, 2020). Since at least to a certain extent antidromic cortical activation could be due to the stimulation of the CST (Devergnas and Wichmann, 2011), it is worth mentioning that a previous study on antidromic cortical activation via stimulation of the CST at the level of the medullary pyramids in cats revealed a complex sequence of quickly changing peaks with a frequency of 500–1000 Hz (Jabbur and Towe, 1961). Yet only initial negative and positive peaks were identified as being of purely antidromic activation. In the text below, by HFO in the context of antidromic activation we mean DBS-evoked high-frequency activity.

On a methodological level, non-invasive EEG technology allows the discrimination of different components of HFO (Klostermann et al., 2000a, 2000b, 1999) which may in turn allow investigation of both antidromic and polysynaptic components of HFO typically associated with HDP activation (Devergnas and Wichmann, 2011). It is also important to note that previous studies directly assessing cortical activation due to STN stimulation have used rather standard techniques for the registration and analysis of neuronal activity with an amplitude of a few microvolts. There were no attempts to specifically analyze low-amplitude HFO in the frequency range $>$ 300 Hz extending potentially to 1 kHz. Our previous results have shown that somatosensory HFO (Waterstraat et al., 2015a) are considerably smaller, being at best only hundreds of nanovolts and thus their detection depends heavily on the use of special EEG amplifiers with very low levels of electronic noise and the application of advanced signal processing (see below).

As mentioned earlier, antidromic stimulation of the cortex should lead to the activation of pyramidal cells in cortical layer V according to anatomical studies in rats (Li et al., 2012). Since these pyramidal cells are large and oriented perpendicular to the surface, the resulting electromagnetic fields should be sufficiently strong to allow even noninvasive detection of weak antidromic activation.

Important to note is that antidromically evoked responses have so far mostly been measured with a limited spatial coverage using either only a few intracortical or scalp EEG electrodes, and therefore a spatial spread of evoked responses (and HFO) is still not known. At the same time, it is known that, apart from the motor cortex, many other areas project to STN including SMA, PMC, and non-motor areas of the frontal cortex (Canteras et al., 1990; Devergnas and Wichmann, 2011; Nambu et al., 1997, 1996). Therefore, cortical activation due to STN stimulation can be best captured with whole-head multichannel EEG and MEG systems, permitting the application of advanced spatial filtering techniques (described below) for the extraction of separate spatial and temporal components of HFO.

Direct recordings of cortical spiking activity due to antidromic cortical activation have been previously performed in 6-OHDA lesioned rodents (Li et al., 2012) and in the non-human primate MPTP model (Johnson et al., 2020). Typical criteria for deciding whether spiking activity is due to antidromic activations were: short latency ($<$3 ms) spikes and low temporal jitter. Neurons classified as being activated antidromically demonstrated firing rates of about 370 Hz (Johnson et al., 2020) which is the frequency range we advocate for the use of HFO as a biomarker of antidromic activation. The presence of HFO might thus be useful for discriminating direct cortical activation from the general excitatory or inhibitory changes due to cortical activation which can also reflect orthodromic effects of STN activation.

Another important aspect of STN-DBS in a primate model (Johnson et al., 2020) was that it strongly attenuated synchronization of spontaneous spiking activity between neurons in M1, and the authors even suggested that such reduced synchronization might be the basis of the therapeutic efficacy of STN-DBS. HFO are manifested not only in relatively sharp spectral peaks but also as a relatively diffuse spectral elevation $>$300 Hz (Fedele et al., 2012). Since local synchronization of spontaneous spiking activity leads to larger measurable electromagnetic fields (Teleńczuk et al., 2015), an attenuation of spatial neuronal synchronization should vice versa result in the attenuation of broadband HFO which could be detected even non-invasively with scalp EEG using appropriate technology (see below).

4.3. Recording high-frequency oscillations – technology and methods

When measured invasively (Baranauskas et al., 2012; Semenova et al., 2021) and non-invasively (Freeman et al., 2003; Pritchard, 1992), the amplitude of neuronal oscillations scales in a relation inversely proportional to the oscillatory frequency. Noteworthy, however, it is not the amplitude itself but the SNR of HFO determining their detectability in recorded data. Here, the SNR is understood as the ratio of signal amplitude and the amplitude of all simultaneously measured activity in the same frequency range. This frequency range can be isolated by band-pass filtering. Yet, the filter passband would unavoidably include HFO and noise activity (of biologic and electronic origin), and filtering might introduce undesirable filtering effects and artifacts (Widmann et al.,

2015; Widmann and Schröger, 2012).

Describing the effective SNR warrants an individual assessment of both constituents, signal and noise. The noise power in the frequency range < 100 Hz is dominated by biological 'background activity' (Scheer et al., 2006), and since also the amplitude of this background activity decreases at higher frequencies, the SNR remains approximately constant until a few hundred Hz (typically <200 Hz depending on modality and measurement technology). In agreement with this reasoning, modeling studies have confirmed the observation that "epileptic" ripple band HFO (80–200 Hz) generated from a cortical region of approx. 1 cm^2 are detectable in conventional surface EEG recordings (von Ellenrieder et al., 2014). Confirmed in the same study, the spatial source resolution of EEG is, however, not constrained by elementary biophysical principles or the adverse skull conductivity but exclusively determined by the SNR: In the complete absence of concurrent signal activity or noise, any signal could be detected independent of its amplitude, and, in a multichannel set-up, be precisely localized. Distinguishing between closely co-localized eCRs thus requires an optimization of the SNR.

Complicating EEG/MEG analysis at frequencies >500 Hz, however, the spectral 1/f trend is superseded by a spectrally flat white noise floor which is composed of sensor noise, noise of the measurement device (Scheer et al., 2006), and - in case of MEG - thermal body noise (Myers et al., 2007; Storm et al., 2019). Using somatosensory HFO ~600 Hz as a model system, their SNR in an individual subject was demonstrated to be directly linked to the noise of the EEG amplifier used in these recordings (Waterstraat et al., 2012). In consequence, usage of low-noise amplifier technology enabled the single-trial detection of somatosensory HFO (Waterstraat et al., 2015a, 2016).

On the numerator of the SNR, HFO signal power is pre-determined by subject and experimental condition. Advantage can, however, be taken from the distributed spatial field of HFO. Depending on its configuration, standard referential or bipolar montages may not provide the optimal SNR. Spatial filtering generalizes the concept of montages to arbitrary channel weightings, and optimal spatial filters can be designed targeting different signal properties such as: mutual independence between sources (ICA) (Hyvärinen and Oja, 2000), the SNR of neuronal oscillations (Nikulin et al., 2011), power or phase coupling (Dähne et al., 2014; Waterstraat et al., 2017), canonical coherence (Vidaurre et al., 2019) or generally non-linear interactions between signals (Idaji et al., 2020).

Spatial filtering with channel weights obtained by Canonical Correlation Average Regression (Fig. 2C; CCAvReg) (Fedele et al., 2013) or

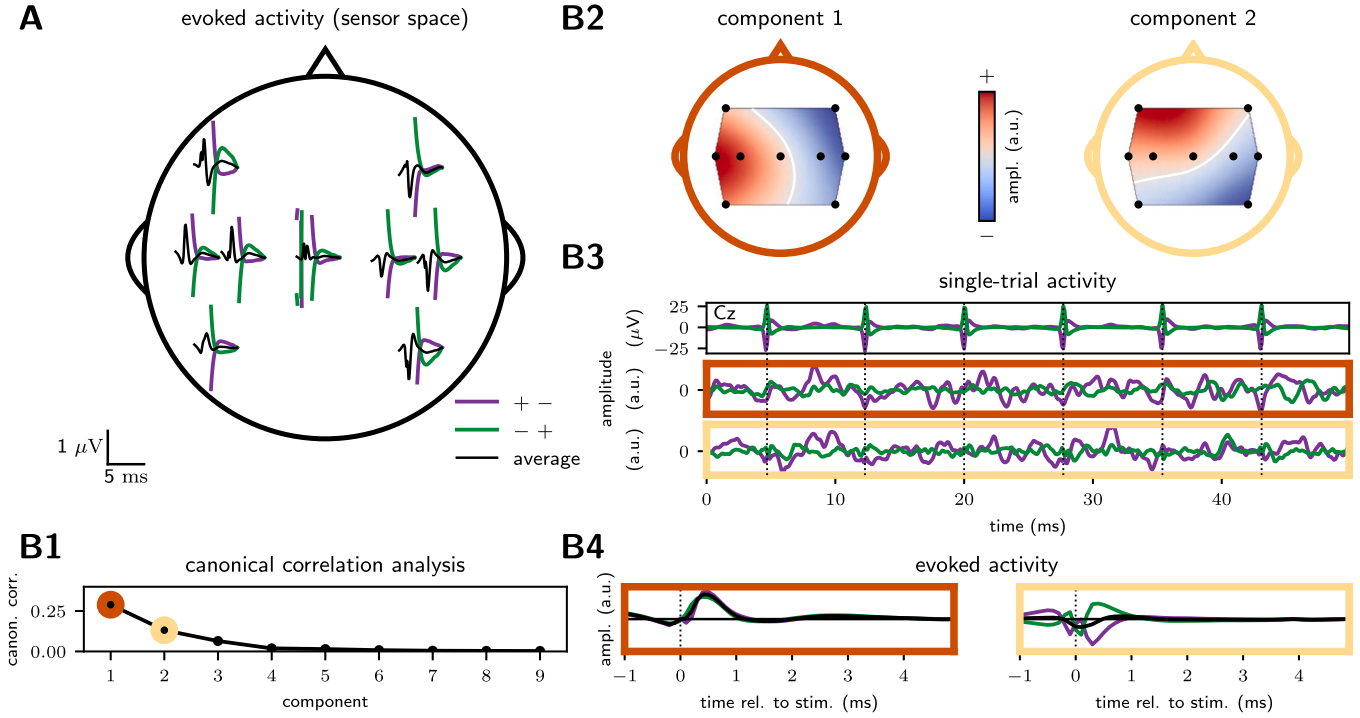

Fig. 3. Short- and medium-latency eCRs evoked by 130 Hz DBS in the left STN enhanced by spatial filtering with Canonical Correlation Average Regression (CCAvReg) after band-pass filtering 300–1200 Hz (1st order IIR filter applied in forward and backward direction). 8-channel low-noise surface EEG obtained from a PD patient with bilaterally implanted depth electrodes in the STN during unilateral left-sided stimulation (lowest contact against 2nd lowest contact; 60 μs stimulus width; 4.6 mA constant current intensity). (A): eCRs recorded by non-invasive surface EEG (average reference) suffer from large electric stimulation artifacts that reverse polarity according to the inversion of the stimulus polarity (purple/green lines). Averaging across an equal number of trials with opposite stimulus polarity cancels the electric stimulus artifact to a large degree. However, due to a possible asymmetry of the electric stimulation artifact in both stimulation conditions, potentially genuine eCRs cannot be safely discerned from spurious components (black lines). (B1–B4): CCAvReg was simultaneously trained on data from both stimulation polarities to extract components with maximum correlation between single-trial responses and their own average. If eCRs are present, this algorithm finds components with maximum eCR contribution while minimizing the contribution of the electric stimulation artifact. (B1): CCAvReg components are sorted according to decreasing canonical correlation coefficients between single-trial responses and average response. The first ('best') and second ('2nd best') component are indicated in ocher and rosy color, respectively. (B2): Spatial patterns of the first (left) and second (right) CCAvReg components. (B3): Continuous data before spatial filtering (top; electrode Cz) and after spatial filtering with the filters of the first (middle row) and second (bottom; rosy color) component. Amplitude is in arbitrary units (a.u.). While data before spatial filtering is strongly affected by the electric stimulus artifact, optimized spatial filtering can almost completely remove it. (B4): In the first CCAvReg component (left), responses have the same polarity despite opposite stimulus polarity, indicating an effective rejection of the stimulus artifact by spatial filtering. The analysis uncovers an early response (<1 ms) followed by a series of medium-latency eCRs of low amplitude. In the second CCA component right, the stimulus artifact appears to be removed incompletely, and, hence, it remains uncertain whether the obtained average component is a genuine eCR. A more systematic investigation of recordings is needed to enable an interpretation of these findings. (For interpretation of the references to color in this figure legend, the reader is referred to the web version of this article.)

the xDAWN algorithm (Rivet et al., 2009) maximizes the correlation of single-trial responses to the average stimulus response and is therefore specifically suited for the analysis of evoked HFO such as conceptualized in the context of STN-DBS. Multiple uncorrelated source components can be extracted simultaneously and are sorted according to their degree of stimulus locking and latencies/phase shifts. Optimal spatial filtering approximately leads to a doubling of the SNR in case of somatosensory HFO (Waterstraat et al., 2015a, 2015b).

Furthermore, spatial filtering methods provide information about the localization of a source component. For every spatial filter, a corresponding activation pattern can be obtained indicating the strength and polarity of the represented source at every sensor (Haufe et al., 2014). This information can in turn be used for improved inverse source reconstruction of the extracted components.

Altogether, a promising recipe (Waterstraat et al., 2015b) for an optimized detection and analysis of HFO is composed of: (I) signal-tailored band-pass filtering in the frequency range of interest, (II) low-noise recording technology, and (III) optimal spatial filtering to utilize and determine the distributed spatial field of HFO sources. An example, applying this analysis recipe to non-invasive surface EEG data during 130 Hz STN-DBS, is given in Fig. 3.

5. Conclusion

The HDP can be characterized anatomically as well as electrophysiologically. In the physiological state the HDP is mainly relevant for sending inhibitory signals to the STN. Anatomical studies indicate a widespread cortical distribution of fibers that project to the STN (Canteras et al., 1990; Nambu et al., 1996). In line with this medium-latency eCR due to STN-DBS exhibit a wide cortical distribution that depends on the stimulated subsection of the STN (Miocinovic et al., 2018). These medium-latency eCR might even serve as potential biomarker for therapeutic effects of STN-DBS. In addition, the connectivity between STN and cortical areas relates to the efficacy of STN-DBS (Akram et al., 2017; Maurice et al., 1998).

We propose that the activation sequence of eCR can be conceptualized as HFO of about 500 Hz for the purpose of signal analysis. However, standard experimental paradigms do not trigger electromagnetic fields as strong as STN-DBS, rendering the non-invasive recording of the eCR-HFO technically challenging. A successful detection of low amplitude HFO requires a recording technology with a low inherent noise level, band-pass filtering in the frequency range of interest, and well adapted spatial filtering. Applying this approach, the SNR can be substantially improved and HFO can even be detected on a single-trial level (Waterstraat et al., 2015b).

Financial disclosures

AS has been serving as a consultant for and received consultant and speaker fees from Medtronic Inc., Boston Scientific and St. Jude Medical/Abbott. BB, GW, SK, GC, VN and EF declare that they have no known competing financial interests or personal relationships that could have appeared to influence the work reported in this paper.

Declaration of Competing Interest

The authors declare that they have no known competing financial interests or personal relationships that could have appeared to influence the work reported in this paper.

Acknowledgements

Funded by the Deutsche Forschungsgemeinschaft (DFG, German Research Foundation) – Project-ID 424778381 – TRR 295. EF gratefully acknowledges support by the Volkswagen Foundation (Lichtenberg program 89387).

References

Akram, H., Sotiropoulos, S.N., Jbabdi, S., Georgiev, D., Mahlknecht, P., Hyam, J., Foltynie, T., Limousin, P., De Vita, E., Jahanshahi, M., Hariz, M., Ashburner, J., Behrens, T., Zrinzo, L., 2017. Subthalamic deep brain stimulation sweet spots and hyperdirect cortical connectivity in Parkinson's disease. NeuroImage 158, 332–345. https://doi.org/10.1016/j.neuroimage.2017.07.012.

Albin, R.L., Young, A.B., Penney, J.B., 1989. The functional anatomy of basal ganglia disorders. Trends Neurosci. 12, 366–375. https://doi.org/10.1016/0166-2236(89)90074-X.

Amunts, K., Lepage, C., Borgeat, L., Mohlberg, H., Dickscheid, T., Rousseau, M.É., Bludau, S., Bazin, P.L., Lewis, L.B., Oros-Peusquens, A.M., Shah, N.J., Lippert, T., Zilles, K., Evans, A.C., 2013. BigBrain: an ultrahigh-resolution 3D human brain model. Science. 340, 1472–1475. https://doi.org/10.1126/science.1235381.

Anderson, R.W., Farokhniaee, A., Gunalan, K., Howell, B., McIntyre, C.C., 2018. Action potential initiation, propagation, and cortical invasion in the hyperdirect pathway during subthalamic deep brain stimulation. Brain Stimul. 11, 1140–1150. https://doi.org/10.1016/j.brs.2018.05.008.

Ashby, P., Paradiso, G., Saint-Cyr, J.A., Chen, R., Lang, A.E., Lozano, A.M., 2001. Potentials recorded at the scalp by stimulation near the human subthalamic nucleus. Clin. Neurophysiol. 112, 431–437. https://doi.org/10.1016/S1388-2457(00)00532-0.

Awad, M.Z., Vaden, R.J., Irwin, Z.T., Gonzalez, C.L., Black, S., Nakhmani, A., Jaeger, B. C., Bentley, J.N., Guthrie, B.L., Walker, H.C., 2021. Subcortical short-term plasticity elicited by deep brain stimulation. Ann. Clin. Transl. Neurol. 8, 1010–1023. https://doi.org/10.1002/ACN3.51275.

Baker, K.B., Montgomery Jr., E.B., Rezai, A.R., Burgess, R., Lüders, H.O., 2002. Subthalamic nucleus deep brain stimulus evoked potentials: physiological and therapeutic implications. Mov. Disord. 17, 969–983. https://doi.org/10.1002/mds.10206.

Baker, S.N., Curio, G., Lemon, R.N., 2003. EEG oscillations at 600 Hz are macroscopic markers for cortical spike bursts. J. Physiol. 550, 529–534. https://doi.org/10.1113/jphysiol.2003.045674.

Baranauskas, G., Maggiolini, E., Vato, A., Angotzi, G., Bonfanti, A., Zambra, G., Spinelli, A., Fadiga, L., 2012. Origins of 1/f2 scaling in the power spectrum of intracortical local field potential. J. Neurophysiol. 107, 984–994. https://doi.org/10.1152/jn.00470.2011.

Bhanpuri, N.H., Bertucco, M., Ferman, D., Young, S.J., Liker, M.A., Krieger, M.D., Sanger, T.D., 2014. Deep brain stimulation evoked potentials may relate to clinical benefit in childhood dystonia. Brain Stimul. 7, 718–726. https://doi.org/10.1016/j.brs.2014.06.003.

Campbell, B.A., Cho, H., Faulhammer, R.M., Hogue, O., Tsai, J.P.-C., Hussain, M.S., Machado, A.G., Baker, K.B., 2021. Stability and effect of Parkinsonian state on deep brain stimulation cortical evoked potentials. Neuromod. https://doi.org/10.1111/NER.13508. E-pub ahead of print.

Canteras, N.S., Shammah-Lagnada, S.J., Silva, B.A., Ricardo, J.A., 1988. Somatosensory inputs to the subthalamic nucleus: a combined retrograde and anterograde horseradish peroxidase study in the rat. Brain Res. 458, 53–64. https://doi.org/10.1016/0006-8993(88)90495-7.

Canteras, N.S., Shammah-Lagnado, S.J., Silva, B.A., Ricardo, J.A., 1990. Afferent connections of the subthalamic nucleus: a combined retrograde and anterograde horseradish peroxidase study in the rat. Brain Res. 513, 43–59. https://doi.org/10.1016/0006-8993(90)91087-W.

Chen, W., de Hemptinne, C., Miller, A.M., Leibbrand, M., Little, S.J., Lim, D.A., Larson, P. S., Starr, P.A., 2020. Prefrontal-subthalamic hyperdirect pathway modulates movement inhibition in humans. Neuron 106, 579–588.e3. https://doi.org/10.1016/j.neuron.2020.02.012.

Chen, Y., Ge, S., Li, Y., Li, N., Wang, J., Wang, X., Li, J., Jing, J., Su, M., Zheng, Z., 2018. Role of the cortico-subthalamic hyperdirect pathway in deep brain stimulation for the treatment of Parkinson disease: a diffusion tensor imaging study. World Neurosurg. 114, e1079–e1085. https://doi.org/10.1016/j.wneu.2018.03.149.

Coudé, D., Parent, A., Parent, M., 2018. Single-axon tracing of the corticosubthalamic hyperdirect pathway in primates. Brain Struct. Funct. 223, 3959–3973. https://doi.org/10.1007/s00429-018-1726-x.

Curio, G., 2000. Linking 600-Hz "spikelike" EEG/MEG wavelets ("ς-bursts") to cellular substrates: concepts and caveats. J. Clin. Neurophysiol. 17, 377. https://doi.org/10.1097/00004691-200007000-00004.

Curio, G., Mackert, B.M., Burghoff, M., Koetitz, R., Abraham-Fuchs, K., Härer, W., 1994. Localization of evoked neuromagnetic 600 Hz activity in the cerebral somatosensory system. Electroencephalogr. Clin. Neurophysiol. 91, 483–487. https://doi.org/10.1016/0013-4694(94)90169-4.

Dähne, S., Meinecke, F.C., Haufe, S., Höhne, J., Tangermann, M., Müller, K.-R., Nikulin, V.V., 2014. SPoC: a novel framework for relating the amplitude of neuronal oscillations to behaviorally relevant parameters. NeuroImage 86, 111–122. https://doi.org/10.1016/j.neuroimage.2013.07.079.

Dejean, C., Hyland, B., Arbuthnott, G., 2009. Cortical effects of subthalamic stimulation correlate with behavioral recovery from dopamine antagonist induced akinesia. Cereb. Cortex 19, 1055–1063. https://doi.org/10.1093/cercor/bhn149.

DeLong, M.R., 1990. Primate models of movement disorders of basal ganglia origin. Trends Neurosci. 13, 281–285. https://doi.org/10.1016/0166-2236(90)90110-V.

Dembek, T.A., Reker, P., Visser-Vandewalle, V., Wirths, J., Treuer, H., Klehr, M., Roediger, J., Dafsari, H.S., Barbe, M.T., Timmermann, L., 2017. Directional DBS increases side-effect thresholds—a prospective, double-blind trial. Mov. Disord. 32, 1380–1388. https://doi.org/10.1002/mds.27093.

Devergnas, A., Wichmann, T., 2011. Cortical potentials evoked by deep brain stimulation in the subthalamic area. Front. Syst. Neurosci. 5, 30. https://doi.org/10.3389/fnsys.2011.00030.

Donoghue, J.P., Kitai, S.T., 1981. A collateral pathway to the neostriatum from corticofugal neurons of the rat sensory-motor cortex: an intracellular HRP study. J. Comp. Neurol. 201, 1–13. https://doi.org/10.1002/cne.902010102.

von Ellenrieder, N., Beltrachini, L., Perucca, P., Gotman, J., 2014. Size of cortical generators of epileptic interictal events and visibility on scalp EEG. NeuroImage 94, 47–54. https://doi.org/10.1016/j.neuroimage.2014.02.032.

Eusebio, A., Pogosyan, A., Wang, S., Averbeck, B., Gaynor, L.D., Cantiniaux, S., Witjas, T., Limousin, P., Azulay, J.-P., Brown, P., 2009. Resonance in subthalamo-cortical circuits in Parkinson's disease. Brain 132, 2139–2150. https://doi.org/10.1093/brain/awp079.

Ewert, S., Plettig, P., Li, N., Chakravarty, M.M., Collins, D.L., Herrington, T.M., Kühn, A. A., Horn, A., 2018. Toward defining deep brain stimulation targets in MNI space: a subcortical atlas based on multimodal MRI, histology and structural connectivity. NeuroImage. https://doi.org/10.1016/j.neuroimage.2017.05.015.

Fedele, T., Scheer, H.J., Waterstraat, G., Telenczuk, B., Burghoff, M., Curio, G., 2012. Towards non-invasive multi-unit spike recordings: mapping 1kHz EEG signals over human somatosensory cortex. Clin. Neurophysiol. 123, 2370–2376. https://doi.org/10.1016/j.clinph.2012.04.028.

Fedele, T., Scheer, H.-J., Burghoff, M., Waterstraat, G., Nikulin, V.V., Curio, G., 2013. Distinction between added-energy and phase-resetting mechanisms in non-invasively detected somatosensory evoked responses. Conf. Proc. IEEE Eng. Med. Biol. Soc. 2013, 1688–1691. https://doi.org/10.1109/EMBC.2013.6609843.

Fedele, T., Scheer, H.J., Burghoff, M., Curio, G., Körber, R., 2015. Ultra-low-noise EEG/MEG systems enable bimodal non-invasive detection of spike-like human somatosensory evoked responses at 1 kHz. Physiol. Meas. 36, 357–368. https://doi.org/10.1088/0967-3334/36/2/357.

Freeman, W.J., Holmes, M.D., Burke, B.C., Vanhatalo, S., 2003. Spatial spectra of scalp EEG and EMG from awake humans. Clin. Neurophysiol. 114, 1053–1068. https://doi.org/10.1016/s1388-2457(03)00045-2.

Giuffrida, R., Li Volsi, G., Maugeri, G., Perciavalle, V., 1985. Influences of pyramidal tract on the subthalamic nucleus in the cat. Neurosci. Lett. 54, 231–235. https://doi.org/10.1016/S0304-3940(85)80084-7.

Gmel, G.E., Hamilton, T.J., Obradovic, M., Gorman, R.B., Single, P.S., Chenery, H.J., Coyne, T., Silburn, P.A., Parker, J.L., 2015. A new biomarker for subthalamic deep brain stimulation for patients with advanced Parkinson's disease—a pilot study. J. Neural Eng. 12, 066013 https://doi.org/10.1088/1741-2560/12/6/066013.

Gradinaru, V., Mogri, M., Thompson, K.R., Henderson, J.M., Deisseroth, K., 2009. Optical deconstruction of Parkinsonian neural circuitry. Science. 324, 354–359. https://doi.org/10.1126/science.1167093.

Gunalan, K., McIntyre, C.C., 2020. Biophysical reconstruction of the signal conduction underlying short-latency cortical evoked potentials generated by subthalamic deep brain stimulation. Clin. Neurophysiol. 131, 542–547. https://doi.org/10.1016/j.clinph.2019.09.020.

Gurney, K., Prescott, T.J., Redgrave, P., 2001. A computational model of action selection in the basal ganglia: a new functional anatomy. Biol. Cybern. 84, 401–410. https://doi.org/10.1007/PL00007984.

Hartmann, C.J., Hirschmann, J., Vesper, J., Wojtecki, L., Butz, M., Schnitzler, A., 2018. Distinct cortical responses evoked by electrical stimulation of the thalamic ventral intermediate nucleus and of the subthalamic nucleus. NeuroImage Clin. 20, 1246–1254. https://doi.org/10.1016/j.nicl.2018.11.001.

Hartmann-von Monakow, K., Akert, K., Künzle, H., 1978. Projections of the precentral motor cortex and other cortical areas of the frontal lobe to the subthalamic nucleus in the monkey. Exp. Brain Res. 33, 395–403. https://doi.org/10.1007/BF00235561.

Hashimoto, I., Mashiko, T., Imada, T., 1996. Somatic evoked high-frequency magnetic oscillations reflect activity of inhibitory interneurons in the human somatosensory cortex. Electroencephalogr. Clin. Neurophysiol. 100, 189–203. https://doi.org/10.1016/0168-5597(95)00244-8.

Haufe, S., Meinecke, F., Görgen, K., Dähne, S., Haynes, J.-D., Blankertz, B., Bießmann, F., 2014. On the interpretation of weight vectors of linear models in multivariate neuroimaging. NeuroImage 87, 96–110. https://doi.org/10.1016/j.neuroimage.2013.10.067.

Haynes, W.I.A., Haber, S.N., 2013. The organization of prefrontal-subthalamic inputs in primates provides an anatomical substrate for both functional specificity and integration: implications for basal ganglia models and deep brain stimulation. J. Neurosci. 33, 4804–4814. https://doi.org/10.1523/JNEUROSCI.4674-12.2013.

Horn, A., Kühn, A.A., 2015. Lead-DBS: a toolbox for deep brain stimulation electrode localizations and visualizations. NeuroImage 107, 127–135. https://doi.org/10.1016/j.neuroimage.2014.12.002.

Howell, B., Isbaine, F., Willie, J.T., Opri, E., Gross, R.E., De Hemptinne, C., Starr, P.A., McIntyre, C.C., Miocinovic, S., 2021. Image-based biophysical modeling predicts cortical potentials evoked with subthalamic deep brain stimulation. Brain Stimul. 14, 549–563. https://doi.org/10.1016/j.brs.2021.03.009.

Hyvärinen, A., Oja, E., 2000. Independent component analysis: algorithms and applications. Neural Netw. 13, 411–430. https://doi.org/10.1016/s0893-6080(00)00026-5.

Idaji, M.J., Müller, K.-R., Nolte, G., Maess, B., Villringer, A., Nikulin, V.V., 2020. Nonlinear interaction decomposition (NID): a method for separation of cross-frequency coupled sources in human brain. NeuroImage 211, 116599. https://doi.org/10.1016/j.neuroimage.2020.116599.

Ikeda, H., Leyba, L., Bartolo, A., Wang, Y., 2002. Synchronized spikes of thalamocortical axonal terminals and cortical neurons are detectable outside the pig brain with MEG. J. Neurophysiol. 87, 626–630. https://doi.org/10.1152/jn.00332.2001.

Irwin, Z.T., Awad, M.Z., Gonzalez, C.L., Nakhmani, A., Bentley, J.N., Moore, T.A., Smithson, K.G., Guthrie, B.L., Walker, H.C., 2020. Latency of subthalamic nucleus deep brain stimulation-evoked cortical activity as a potential biomarker for postoperative motor side effects. Clin. Neurophysiol. 131, 1221–1229. https://doi.org/10.1016/j.clinph.2020.02.021.

Jabbur, S.J., Towe, A.L., 1961. Analysis of the antidromic cortical response following stimulation at the medullary pyramids. J. Physiol. 155, 148–160. https://doi.org/10.1113/jphysiol.1961.sp006619.

Johnson, L.A., Wang, J., Nebeck, S.D., Zhang, J., Johnson, M.D., Vitek, J.L., 2020. Direct activation of primary motor cortex during subthalamic but not pallidal deep brain stimulation. J. Neurosci. 40, 2166–2177. https://doi.org/10.1523/JNEUROSCI.2480-19.2020.

Kita, T., Kita, H., 2012. The subthalamic nucleus is one of multiple innervation sites for long-range corticofugal axons: a single-axon tracing study in the rat. J. Neurosci. 32, 5990–5999. https://doi.org/10.1523/JNEUROSCI.5717-11.2012.

Kitai, S.T., Deniau, J.M., 1981. Cortical inputs to the subthalamus: intracellular analysis. Brain Res. 214, 411–415. https://doi.org/10.1016/0006-8993(81)91204-x.

Klostermann, F., Nolte, G., Curio, G., 1999. Multiple generators of 600 Hz wavelets in human SEP unmasked by varying stimulus rates. Neuroreport 10, 1625–1629. https://doi.org/10.1097/00001756-199906030-00001.

Klostermann, F., Funk, T., Vesper, J., Siedenberg, R., Curio, G., 2000a. Double-pulse stimulation dissociates intrathalamic and cortical high-frequency (>400Hz) SEP components in man. Neuroreport 11, 1295–1299. https://doi.org/10.1097/00001756-200004270-00030.

Klostermann, F., Funk, T., Vesper, J., Siedenberg, R., Curio, G., 2000b. Propofol narcosis dissociates human intrathalamic and cortical high-frequency (>400 Hz) SEP components. Neuroreport 11, 2607–2610. https://doi.org/10.1097/00001756-200008030-00051.

Kumaravelu, K., Oza, C.S., Behrend, C.E., Grill, W.M., 2018. Model-based deconstruction of cortical evoked potentials generated by subthalamic nucleus deep brain stimulation. J. Neurophysiol. 120, 662–680. https://doi.org/10.1152/jn.00862.2017.

Künzle, H., 1978. An autoradiographic analysis of the efferent connections from premotor and adjacent prefrontal regions (areas 6 and 9) in *Macaca fascicularis*. Brain Behav. Evol. 15, 185–209. https://doi.org/10.1159/000123779.

Kuriakose, R., Saha, U., Castillo, G., Udupa, K., Ni, Z., Gunraj, C., Mazzella, F., Hamani, C., Lang, A.E., Moro, E., Lozano, A.M., Hodaie, M., Chen, R., 2010. The nature and time course of cortical activation following subthalamic stimulation in Parkinson's disease. Cereb. Cortex 20, 1926–1936. https://doi.org/10.1093/cercor/bhp269.

Li, Q., Ke, Y., Chan, D.C.W., Qian, Z.-M., Yung, K.K.L., Ko, H., Arbuthnott, G.W., Yung, W.-H., 2012. Therapeutic deep brain stimulation in Parkinsonian rats directly influences motor cortex. Neuron 76, 1030–1041. https://doi.org/10.1016/j.neuron.2012.09.032.

Li, S., Arbuthnott, G.W., Jutras, M.J., Goldberg, J.A., Jaeger, D., 2007. Resonant antridromic cortical circuit activation as a consequence of high-frequency subthalamic deep brain stimulation. J. Neurophysiol. 98, 3525–3537. https://doi.org/10.1152/jn.00808.2007.

Limousin, P., Brown, P., Marsden, J., Defebvre, L., Rothwell, J., 1998. Evoked potentials from subthalamic nucleus, internal pallidum and thalamic stimulation in Parkinsonian and postural tremor patients. J. Physiol. 509P, 176P–177P. https://doi.org/10.1111/j.1469-7793.1998.tb00048.x.

MacKinnon, C.D., Webb, R.M., Silberstein, P., Tisch, S., Asselman, P., Limousin, P., Rothwell, J.C., 2005. Stimulation through electrodes implanted near the subthalamic nucleus activates projections to motor areas of cerebral cortex in patients with Parkinson's disease. Eur. J. Neurosci. 21, 1394–1402. https://doi.org/10.1111/j.1460-9568.2005.03952.x.

Mahlknecht, P., Akram, H., Georgiev, D., Tripoliti, E., Candelario, J., Zacharia, A., Zrinzo, L., Hyam, J., Hariz, M., Foltynie, T., Rothwell, J.C., Limousin, P., 2017. Pyramidal tract activation due to subthalamic deep brain stimulation in Parkinson's disease: pyramidal tract activation due to STN-DBS in PD. Mov. Disord. 32, 1174–1182. https://doi.org/10.1002/mds.27042.

Maurice, N., Deniau, J.-M., Glowinski, J., Thierry, A.-M., 1998. Relationships between the prefrontal cortex and the basal ganglia in the rat: physiology of the corticosubthalamic circuits. J. Neurosci. 18, 9539–9546. https://doi.org/10.1523/jneurosci.18-22-09539.1998.

Meola, A., Yeh, F.-C., Fellows-Mayle, W., Weed, J., Fernandez-Miranda, J.C., 2016. Human connectome-based Tractographic atlas of the brainstem connections and surgical approaches. Neurosurg. 79, 437–455. https://doi.org/10.1227/NEU.0000000000001224.

Middlebrooks, E.H., Domingo, R.A., Vivas-Buitrago, T., Okromelidze, L., Tsuboi, T., Wong, J.K., Eisinger, R.S., Almeida, L., Burns, M.R., Horn, A., Uitti, R.J., Wharen, R. E., Holanda, V.M., Grewal, S.S., 2020. Neuroimaging advances in deep brain stimulation: review of indications, anatomy, and brain connectomics. Am. J. Neuroradiol. https://doi.org/10.3174/ajnr.A6693.

Miocinovic, S., de Hemptinne, C., Chen, W., Isbaine, F., Willie, J.T., Ostrem, J.L., Starr, P. A., 2018. Cortical potentials evoked by subthalamic stimulation demonstrate a short latency hyperdirect pathway in humans. J. Neurosci. 38, 9129–9141. https://doi.org/10.1523/JNEUROSCI.1327-18.2018.

Myers, W., Slichter, D., Hatridge, M., Busch, S., Mößle, M., McDermott, R., Trabesinger, A., Clarke, J., 2007. Calculated signal-to-noise ratio of MRI detected with SQUIDs and Faraday detectors in fields from 10μT to 1.5T. J. Magn. Reson. 186, 182–192. https://doi.org/10.1016/j.jmr.2007.02.007.

Nambu, A., 2005. A new approach to understand the pathophysiology of Parkinson's disease. J. Neurol. 252, iv1–iv4. https://doi.org/10.1007/s00415-005-4002-y.

Nambu, A., Takada, M., Inase, M., Tokuno, H., 1996. Dual somatotopical representations in the primate subthalamic nucleus: evidence for ordered but reversed body-map transformations from the primary motor cortex and the supplementary motor area. J. Neurosci. 16, 2671–2683. https://doi.org/10.1523/JNEUROSCI.16-08-02671.1996.

Nambu, A., Tokuno, H., Inase, M., Takada, M., 1997. Corticosubthalamic input zones from forelimb representations of the dorsal and ventral divisions of the premotor cortex in the macaque monkey: comparison with the input zones from the primary motor cortex and the supplementary motor area. Neurosci. Lett. 239, 13–16. https://doi.org/10.1016/S0304-3940(97)00877-X.

Ni, Z., Kim, S.J., Phielipp, N., Ghosh, S., Udupa, K., Gunraj, C.A., Saha, U., Hodaie, M., Kalia, S.K., Lozano, A.M., Lee, D.J., Moro, E., Fasano, A., Hallett, M., Lang, A.E., Chen, R., 2018. Pallidal deep brain stimulation modulates cortical excitability and plasticity. Ann. Neurol. 83, 352–362. https://doi.org/10.1002/ana.25156.

Nikolov, P., Heil, V., Hartmann, C.J., Ivanov, N., Slotty, P.J., Vesper, J., Schnitzler, A., Groiss, S.J., 2021. Motor evoked potentials improve targeting in deep brain stimulation surgery. Neuromod. https://doi.org/10.1111/NER.13386.

Nikulin, V.V., Nolte, G., Curio, G., 2011. A novel method for reliable and fast extraction of neuronal EEG/MEG oscillations on the basis of spatio-spectral decomposition. NeuroImage 55, 1528–1535. https://doi.org/10.1016/j.neuroimage.2011.01.057.

Ozturk, M., Viswanathan, A., Sheth, S.A., Ince, N.F., 2021. Electroceutically induced subthalamic high-frequency oscillations and evoked compound activity may explain the mechanism of therapeutic stimulation in Parkinson's disease. Commun. Biol. 41 (4), 1–14. https://doi.org/10.1038/s42003-021-01915-7.

Petersen, M.V., Lund, T.E., Sunde, N., Frandsen, J., Rosendal, F., Juul, N., Østergaard, K., 2017. Probabilistic versus deterministic tractography for delineation of the cortico-subthalamic hyperdirect pathway in patients with Parkinson disease selected for deep brain stimulation. J. Neurosurg. 126, 1657–1668. https://doi.org/10.3171/2016.4.JNS1624.

Plantinga, B.R., Roebroeck, A., Kemper, V.G., Uludağ, K., Melse, M., Mai, J., Kuijf, M.L., Herrler, A., Jahanshahi, A., ter Haar Romeny, B.M., 2016. Ultra-high field MRI post mortem structural connectivity of the human subthalamic nucleus, substantia nigra, and globus pallidus. Front. Neuroanat. 10, 66. https://doi.org/10.3389/fnana.2016.00066.

Porter, R., Sanderson, J.H., 1964. Antidromic cortical response to pyramidal-tract stimulation in the rat. J. Physiol. 170, 355–370. https://doi.org/10.1113/jphysiol.1964.sp007336.

Pritchard, W.S., 1992. The brain in fractal time: 1/f-like power spectrum scaling of the human electroencephalogram. Int. J. Neurosci. 66, 119–129. https://doi.org/10.3109/00207459208999796.

Rivet, B., Souloumiac, A., Attina, V., Gibert, G., 2009. xDAWN algorithm to enhance evoked potentials: application to brain–computer interface. IEEE Trans. Biomed. Eng. 56, 2035–2043. https://doi.org/10.1109/TBME.2009.2012869.

Romeo, A., Dubuc, D.M., Gonzalez, C.L., Patel, N.D., Cutter, G., Delk, H., Guthrie, B.L., Walker, H.C., 2019. Cortical activation elicited by subthalamic deep brain stimulation predicts postoperative motor side effects. Neuromod. 22, 456–464. https://doi.org/10.1111/ner.12901.

Rouzaire-Dubois, B., Scarnati, E., 1985. Bilateral corticosubthalamic nucleus projections: an electrophysiological study in rats with chronic cerebral lesions. Neurosci. 15, 69–79. https://doi.org/10.1016/0306-4522(85)90124-1.

Sanders, T.H., Jaeger, D., 2016. Optogenetic stimulation of cortico-subthalamic projections is sufficient to ameliorate bradykinesia in 6-OHDA lesioned mice. Neurobiol. Dis. 95, 225–237. https://doi.org/10.1016/j.nbd.2016.07.021.

Scheer, H.J., Sander, T., Trahms, L., 2006. The influence of amplifier, interface and biological noise on signal quality in high-resolution EEG recordings. Physiol. Meas. 27, 109–117. https://doi.org/10.1088/0967-3334/27/2/002.

Semenova, U., Popov, V., Tomskiy, A., Shaikh, A.G., Sedov, A., 2021. Pallidal 1/f asymmetry in patients with cervical dystonia. Eur. J. Neurosci. 53 (7), 2214–2219. https://doi.org/10.1111/ejn.14729.

Shils, J., Kochanski, R.B., Borghei, A., Candocia, A., Pal, G.D., Afshari, M., Verhagen, L. M., Sani, S., 2021. Motor evoked potential recordings during segmented deep brain stimulation—a feasibility study. Oper. Neurosurg. 00, 1–7. https://doi.org/10.1093/ons/opaa414.

Sinclair, N.C., McDermott, H.J., Bulluss, K.J., Fallon, J.B., Perera, T., Xu, S.S., Brown, P., Thevathasan, W., 2018. Subthalamic nucleus deep brain stimulation evokes resonant neural activity. Ann. Neurol. 83, 1027–1031. https://doi.org/10.1002/ana.25234.

Sinclair, N.C., McDermott, H.J., Fallon, J.B., Perera, T., Brown, P., Bulluss, K.J., Thevathasan, W., 2019. Deep brain stimulation for Parkinson's disease modulates high-frequency evoked and spontaneous neural activity. Neurobiol. Dis. 130, 104522 https://doi.org/10.1016/J.NBD.2019.104522.

Storm, J.-H., Hömmen, P., Höfner, N., Körber, R., 2019. Detection of body noise with an ultra-sensitive SQUID system. Meas. Sci. Technol. 30, 125103 https://doi.org/10.1088/1361-6501/ab3505.

Teleńczuk, B., Baker, S.N., Herz, A.V.M., Curio, G., 2011. High-frequency EEG covaries with spike burst patterns detected in cortical neurons. J. Neurophysiol. 105, 2951–2959. https://doi.org/10.1152/jn.00327.2010.

Teleńczuk, B., Baker, S.N., Kempter, R., Curio, G., 2015. Correlates of a single cortical action potential in the epidural EEG. NeuroImage 109, 357–367. https://doi.org/10.1016/j.neuroimage.2014.12.057.

Teleńczuk, B., Kempter, R., Curio, G., Destexhe, A., 2017. Refractoriness accounts for variable spike Burst responses in somatosensory cortex. eNeuro 4, 1–17. https://doi.org/10.1523/ENEURO.0173-17.2017.

Tisch, S., Rothwell, J.C., Zrinzo, L., Bhatia, K.P., Hariz, M., Limousin, P., 2008. Cortical evoked potentials from pallidal stimulation in patients with primary generalized dystonia: cortical evoked potentials from GPi DBS. Mov. Disord. 23, 265–273. https://doi.org/10.1002/mds.21835.

Vidaurre, C., Nolte, G., de Vries, I.E.J., Gómez, M., Boonstra, T.W., Müller, K.-R., Villringer, A., Nikulin, V.V., 2019. Canonical maximization of coherence: a novel tool for investigation of neuronal interactions between two datasets. NeuroImage 201, 116009. https://doi.org/10.1016/j.neuroimage.2019.116009.

Walker, H.C., Huang, H., Gonzalez, C.L., Bryant, J.E., Killen, J., Cutter, G.R., Knowlton, R.C., Montgomery, E.B., Guthrie, B.L., Watts, R.L., 2012a. Short latency activation of cortex during clinically effective subthalamic deep brain stimulation for Parkinson's disease. Mov. Disord. 27, 864–873. https://doi.org/10.1002/mds.25025.

Walker, H.C., Huang, H., Gonzalez, C.L., Bryant, J.E., Killen, J., Knowlton, R.C., Montgomery Jr., E.B., Cutter, G.C., Yildirim, A., Guthrie, B.L., Watts, R.L., 2012b. Short latency activation of cortex by clinically effective thalamic brain stimulation for tremor. Mov. Disord. 27, 1404–1412. https://doi.org/10.1002/mds.25137.

Waterstraat, G., Teleńczuk, B., Burghoff, M., Fedele, T., Scheer, H.J., Curio, G., 2012. Are high-frequency (600 Hz) oscillations in human somatosensory evoked potentials due to phase-resetting phenomena? Clin. Neurophysiol. 123, 2064–2073. https://doi.org/10.1016/j.clinph.2012.03.013.

Waterstraat, G., Burghoff, M., Fedele, T., Nikulin, V., Scheer, H.J., Curio, G., 2015a. Non-invasive single-trial EEG detection of evoked human neocortical population spikes. NeuroImage 105, 13–20. https://doi.org/10.1016/j.neuroimage.2014.10.024.

Waterstraat, G., Fedele, T., Burghoff, M., Scheer, H.-J., Curio, G., 2015b. Recording human cortical population spikes non-invasively–An EEG tutorial. J. Neurosci. Methods 250, 74–84. https://doi.org/10.1016/j.jneumeth.2014.08.013.

Waterstraat, G., Scheuermann, M., Curio, G., 2016. Non-invasive single-trial detection of variable population spike responses in human somatosensory evoked potentials. Clin. Neurophysiol. 127, 1872–1878. https://doi.org/10.1016/j.clinph.2015.12.005.

Waterstraat, G., Curio, G., Nikulin, V.V., 2017. On optimal spatial filtering for the detection of phase coupling in multivariate neural recordings. NeuroImage 157, 331–340. https://doi.org/10.1016/j.neuroimage.2017.06.025.

Waterstraat, G., Körber, R., Storm, J.H., Curio, G., 2021. Noninvasive neuromagnetic single-trial analysis of human neocortical population spikes. Proc. Natl. Acad. Sci. U. S. A. 118, 2017401118. https://doi.org/10.1073/pnas.2017401118.

Widmann, A., Schröger, E., 2012. Filter effects and filter artifacts in the analysis of electrophysiological data. Front. Psychol. 3, 233. https://doi.org/10.3389/fpsyg.2012.00233.

Widmann, A., Schröger, E., Maess, B., 2015. Digital filter design for electrophysiological data–a practical approach. J. Neurosci. Methods 250, 34–46. https://doi.org/10.1016/j.jneumeth.2014.08.002.